Scientific Research Publishing

Developing Three-Dimensional Beamshaping Techniques on Volumetric Random Arrays to Suppress Array Sidelobes

Shihyuan Yeh

Department of Electrical and Computer Engineering, Texas A&M University, College Station, TX,
United States of America
Email: steven.yeh66@gmail.com

Abstract

This paper proposes a three-dimensional (3-D) amplitude tapering technique on volumetric random arrays to minimize array sidelobes and emulate phased array operations on mobile platforms. Our ultimate goal is to realize wireless phased array applications carried out by mobile platforms; in this paper, we focus on the development of collaborative beamforming algorithms. This beamshaping technique mitigates the discontinuity of the current distribution along the array aperture and lower array sidelobe level (SLL) by specially paying attention to the array element's depth deviation. In this work, step by step amplitude tapering procedures are clearly illustrated. Further, a reconfigurable phased array with sixteen patch antennas is tested to verify the fidelity of the 3-D beamshaping algorithm. Measured and simulated radiation patterns are benchmarked to evaluate the sidelobe suppression results, and the best sidelobe suppressed region is around the array's main beam.

Keywords

Amplitude Tapering, Antenna Arrays, Array Beamforming, Array Beamshaping, Mobile Platforms, Random Array, Reconfigurable Array, Sidelobe Level, Unmanned Aerial Vehicle

1. Introduction

Phased array operations on mobile platforms have been a topic of interest for many years. The mobile platforms may be swarms of unmanned aerial vehicles (UAVs), constellation of satellites, group of cars, fleets of ships, or any number of other spatially distributed surrogates that are in a non-uniform configuration

with a geometric morphology that changes over time. **Figure 1** gives an imaginary picture of a wireless phased array beamforming system implemented by drones. To realize this wireless array system, the practical challenges associated with wireless synchronization [1] [2], localization, and coordination of dynamic beamforming and beamshaping methodologies [3] [4] [5] must be overcome. Although many techniques need to be established to successfully implement a wireless phased array system, this work primarily focuses on the development of three-dimensional (3-D) beamshaping techniques especially for array with a small number of elements while providing a low sidelobe level (SLL).

In practice, high-amplitude sidelobes are undesirable because of interferences in wireless communication systems and target ambiguities in radar identifications. One way to lower the overall sidelobes is to distribute antennas stochastically [6]. The aperiodic spacing of the swarm effectively diminishes the grating lobes and reduces SLL beyond what is possible in a structured lattice of radiators. Stochastic antenna positions are expected to provide destructive superposition of signals everywhere except the array's main beam. A principal advantage of the random topology is that all elements radiate at full power while keeping a low SLL without any compromise of power degrade. In fact, the reduced SLL is proportional to the array element N [6] [7]; the more antennas (N) are deployed in an array, the lower the SLL and the easier it is to mitigate the array sidelobes. For applications with a relatively small number of array elements, sidelobe cancellation effects are trivial; therefore, applying additional tapered weighting along the aperture illumination to substantially reduce SLL is inevitable.

Many researchers have conducted comprehensive efforts on amplitude tapering for one-dimensional (1-D) and two-dimensional (2-D) arrays [8] [9]. Nonetheless, a 3-D amplitude tapering method is still not widely reported in the literature. A 3-D amplitude tapering algorithm [10] designed for volumetric random arrays is investigated in this work, and the proposed method specifically pays attention to the discrepancies of the array depth. There is little experimental validation of volumetric random arrays, and this work seeks to advance the capabilities of spatially distributed antenna systems. This work adopts concepts from volumetric random arrays to address both the lack of periodicity and the

Figure 1. A wireless phased array beamforming system carried out by drones.

geometric morphing of the swarming cluster over time. It is therefore not the explicit purpose of this work to create a random array, but simply to approximate the swarming behavior of a cluster of intelligent systems as a random process that results in an array with unconstrained element spacing. It is possible to extend this analysis beyond the randomized positions to include orientation (yaw, pitch, and roll) and advanced beamforming operations such as nulling and beamshaping. However, it is important to first demonstrate the basic capabilities of such an array using antennas with fundamentally linear polarized properties. The array in this work is composed of sixteen vertically polarized patch antennas. The patches are intended to represent platforms with directional radiation properties.

2. 3-D Amplitude Tapering Procedures

A 3-D amplitude tapering conduct is advisable to further reduce SLL for volumetric random arrays with a small number of N. Step-by-step procedures are elaborated in this section. In Figure 2, the test array consisted of sixteen patch antennas ($N = 16$) was spatially and stochastically displaced.
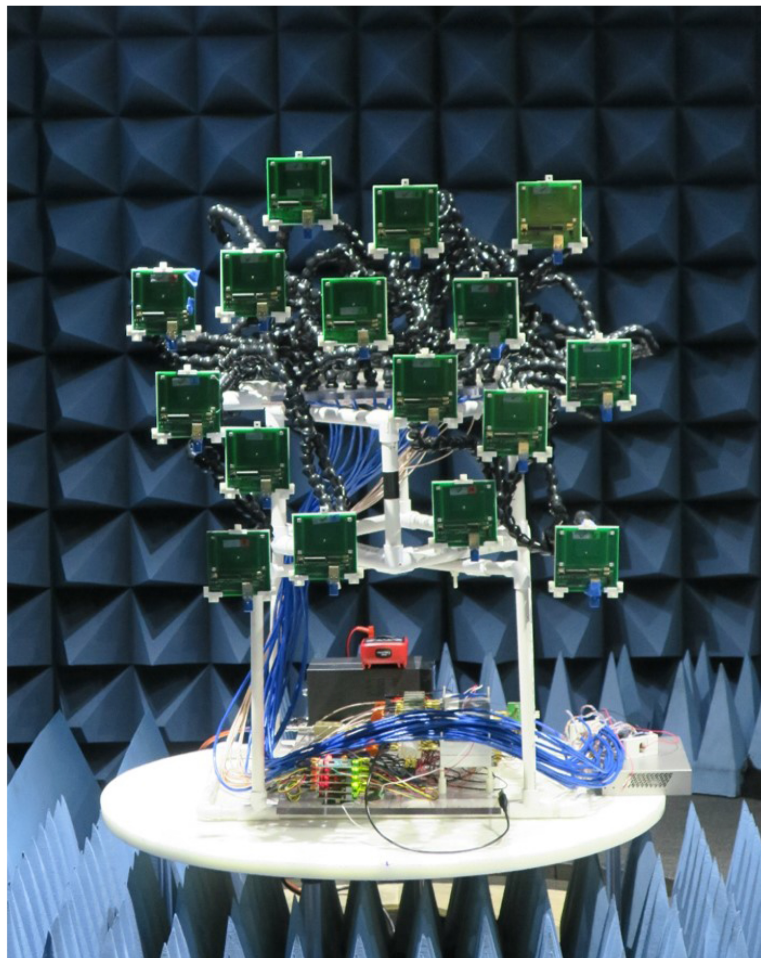

Figure 2. The sixteen-element volumetric random array in the anechoic chamber.

2.1. Beamforming and Phase Optimization

The first step is to steer the array's main beam to the scan angle (θ_s, ϕ_s) and creating the scan angle vector $\bar{S}$ by

$$\bar{S} = \hat{x}\sin\theta_s\cos\phi_s + \hat{y}\sin\theta_s\sin\phi_s + \hat{z}\cos\theta_s. \tag{1}$$

The position of each antenna is denoted as a position vector $\bar{P}$. The progressive length delay from the array scan is calculated by dot product the $\bar{P}$ and $\bar{S}$. In this way, the distance phases [3] of each array element are derived thereafter with the known free-space wavelength. Due to the antenna couplings, an extra phase optimization step potentially increases the phase accuracy.

2.2. Define the Array Aperture

To assign precise current distribution to each array element, it is essential to define the array aperture and identify the aperture origin (AO). **Figure 3** depicts sixteen array elements ($N = 16$) projected onto the array aperture (S'), and each antenna is indicated as antenna element number n, where $n = 1, 2, \cdots, N$. The $\bar{u}$ and $\bar{v}$ are reference vectors, which are horizontally and vertically parallel to S', respectively. The array aperture is a normalized plane, which is perpendicular to the scan angle vector $\bar{S}$, and the array aperture encloses all projected antennas. The AO is located at the center of the array aperture, and it may not be the same as the origin of the coordinate system, keeping in mind that the array aperture implicitly changes with the array scan angle.
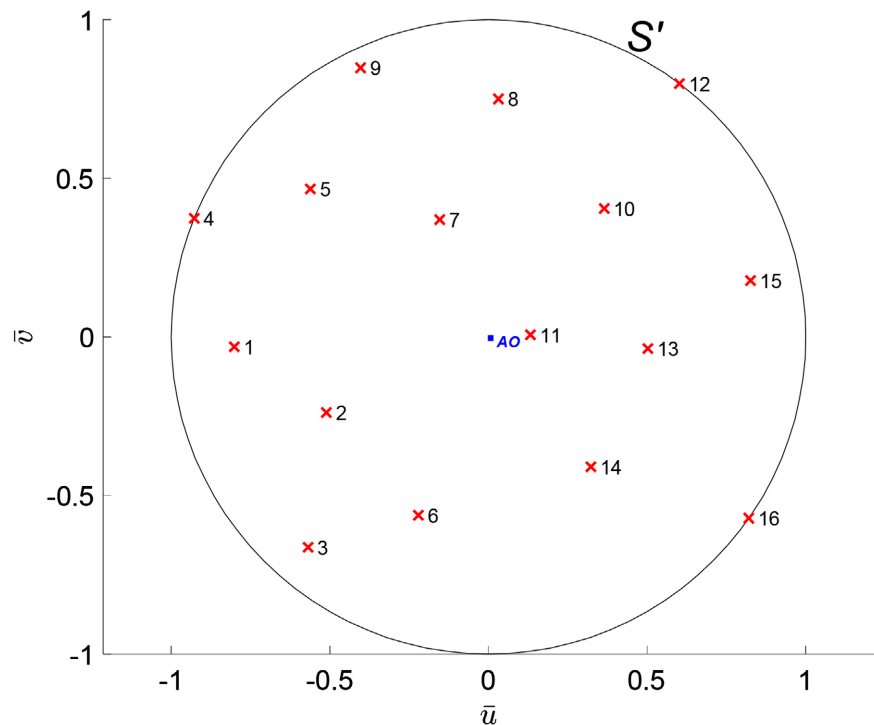

Figure 3. Distribution of sixteen array elements (red cross) projected on the array aperture.

2.3. Amplitude Tapering

There are three kinds of tapering approaches that are utilized in beamshaping operations, and they are radial, horizontal, and vertical tapering. For applications providing azimuth (AZ) and elevation (EL) scan, the current distribution is tapered horizontally and vertically along the array aperture, respectively. Likewise, for 3π ($-\pi \leq$ AZ $\leq \pi$, $0 \leq$ EL $\leq \pi$) scan volume, the antenna excitation is tapered according to the radial distance. The horizontal tapering technique is demonstrated in this work for illustration purpose, and the reference vector $\bar{u}$ is essential to establish by

$$\bar{u}(x, y, z) = \cos\theta_s \cos\phi_s + \cos\theta_s \sin\phi_s - \sin\theta_s, \tag{2}$$

where $\bar{u}$ is a unit vector that is horizontally parallel to S' and orthogonal to $\bar{S}$. Under this circumstance, array elements are projected onto $\bar{u}$ (as shown in **Figure 4**), and each antenna's relative distance to the AO is resolved. In this case, the array aperture is shifted to accommodate for the utmost left and right projected antennas. Making use of the relative distance in $\bar{u}$, the tapering amplitude for each array antenna is obtained accordingly.

2.4. Amplitude Mapping and Averaging

The binomial coefficients (1, 6, 15, 20, 15, 6, 1) are deployed to taper the current amplitudes along the array aperture, and the normalized binomial coefficients are shown as the blue curve in **Figure 5**. Mapping each array element to the binomial curve depends upon the relative distance derived in the previous step.
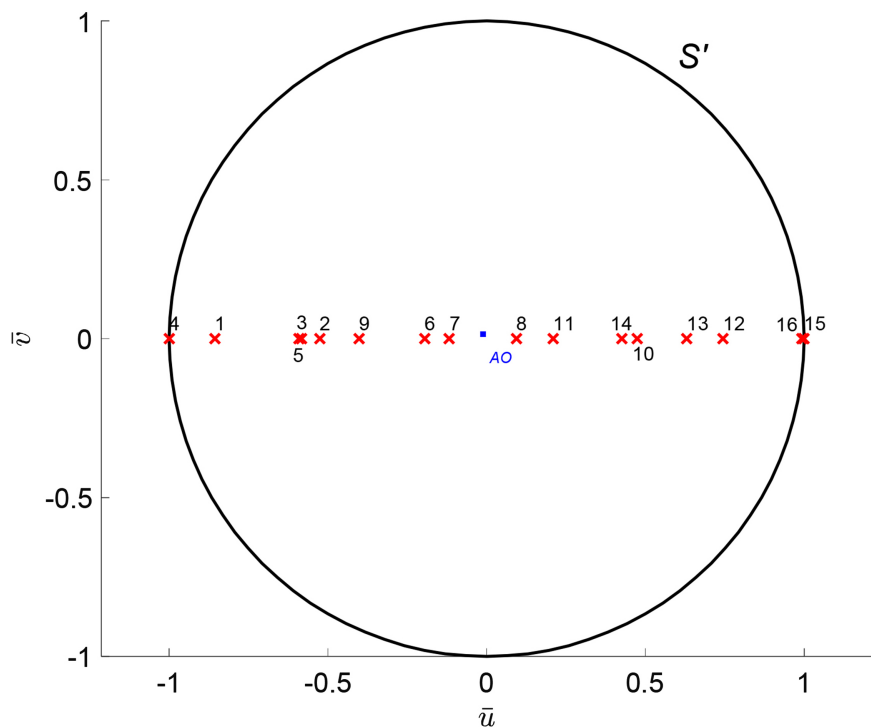

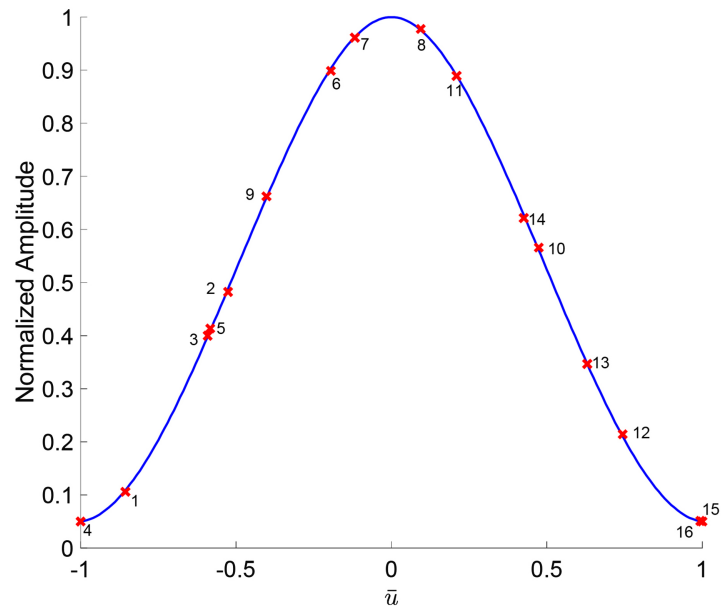**Figure 4.** Sixteen array elements (red cross) projected on the $\bar{u}$.

Figure 5. Sixteen array elements map to the normalized amplitude tapering curve (blue curve).

An evenly and symmetrically distributed current along the array aperture results in a lowest SLL outcome. However, if partial antennas are overlapped or located closely, it creates spike amplitude, which is deviated from the ideally binomial curve. Thus, it is necessary to average the amplitudes to alleviate the spike amplitude. **Figure 6** summarizes the results of amplitude averaging for proximity antennas. For example, elements #3 and #5 are close to each other; therefore, both of its amplitudes are divided by 2. Similarly, the amplitudes for elements #15 and #16 are averaged.

2.5. Depth Gain

One major difference compared volumetric arrays to linear or planar arrays is the depth deviation. The depth is defined as the shortest distance between array elements to the array aperture. As antenna radiates electromagnetic wave, the wave reduces its power density as it propagates through free space. As a result, antennas with farther depth need to reimburse more excitation power to even the propagation loss. Once the depth of each array element is acquired, array antennas are mapped to the propagation-loss curve, as shown in **Figure 7**. Subsequently, the loss from the depth is added back to each antenna; therefore, the discontinuity of the current distribution along the array aperture is flatted by this process.

3. Experiment

The fidelity of the 3-D beamshaping algorithm is examined by implementing pattern measurement campaigns in the far-field anechoic chamber (located at the Electromagnetics and Microwave Laboratory, Department of Electrical and

Computer Engineering, Texas A&M University) to reduce multipath reflections and replicate a free space environment. When considering the characteristics of the mobile platform criteria, the volumetric random array becomes a proper candidate. In this work, the volumetric random array is demonstrated by the reconfigurable phased array [11] shown in **Figure 8**.
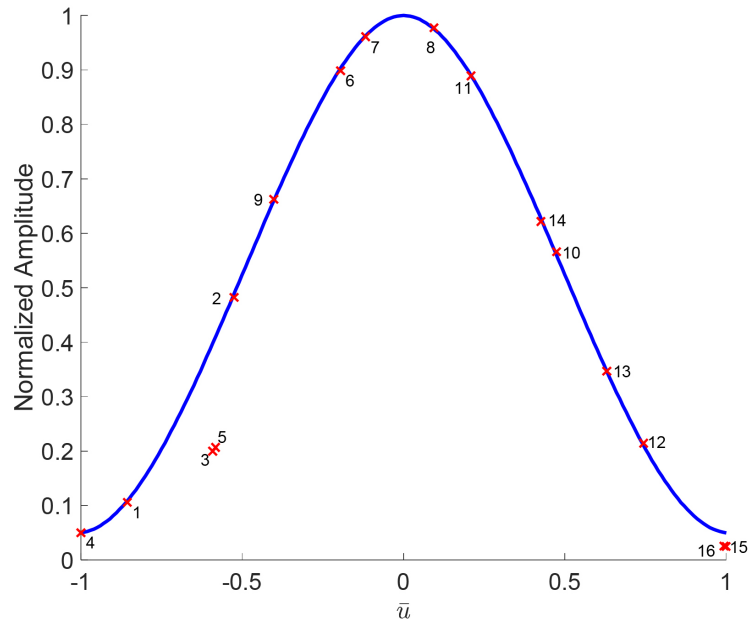
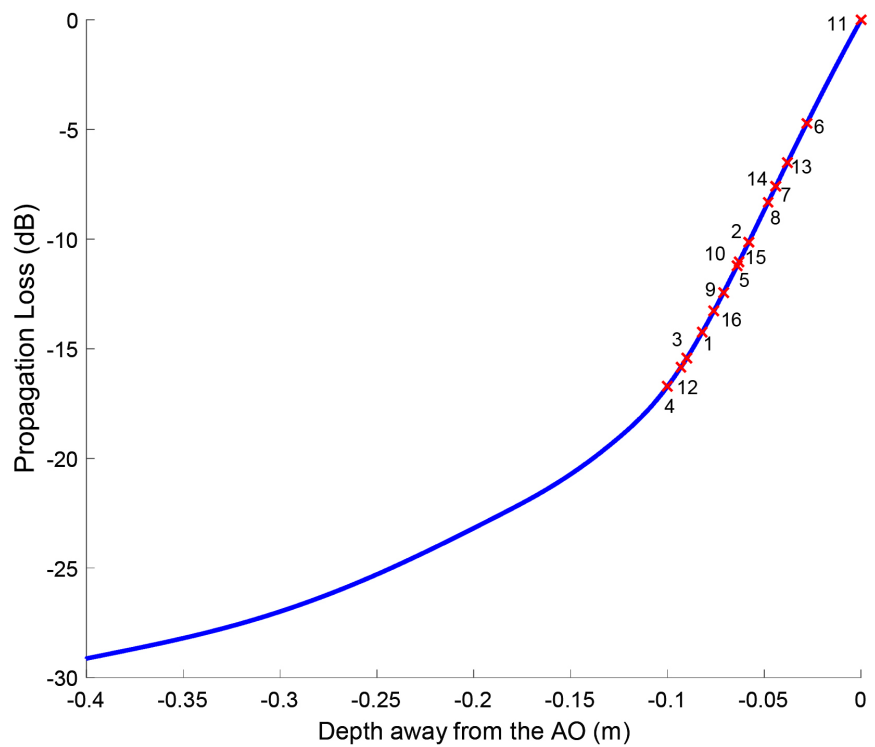**Figure 6.** Amplitude averaging for proximity antennas.

Figure 7. Propagation loss of an antenna from 0 m to 0.5 m.

Figure 8. The photograph of the sixteen-element experimental array displaced in the anechoic chamber.

Sixteen vertical-polarized patch antennas ($N = 16$) are acted as the mobile radiators, and each antenna is positioned by moving the flexible arms (made from acetal copolymer) to the designated location. Array elements are distributed stochastically in a volumetric formation, and the maximum depth differences (along the array's broadside direction) among antennas are limited to one free-space wavelength ($\leq$125 mm) of the operating frequency (2.4 GHz) for the sake of tapering performance. Array antennas are aligned upright (y-polarized) and orthogonal/facing to the z-axis to provide linearly polarized characteristic. The positions of the array antennas are obtained and recorded by the spatial recognition system [11]. In addition, the obtained positions are fed to the ANSYS HFSS simulator, as shown in Figure 9 and Figure 10. The array simulations are carried out thereafter the pattern measurements.

The microstrip patch antenna acting as the array element has linearly polarized characteristic. The patch is well designed to operate at 2.4 GHz with approximately 50 Ω input impedance; therefore, no extra impedance matching network needs to be added, which significantly reduces the complexity and cost of the antenna element. These antennas are fabricated on 62 mil (1.57 mm) thick FR4 ($\epsilon_r = 4.4$) and have a width $w = 38$ mm and resonant length $L = 28$ mm. The SMA probe feed is placed at a distance of 6 mm from the patch edge. Figure 11 shows the measured VSWR and input impedance of the patch antenna from 2 GHz to 3 GHz. The antenna has a 2:1 VSWR bandwidth of 60 MHz (from 2.365 GHz to 2.425 GHz) centered at 2.395 GHz. Figure 12 shows the measured radiation pattern at 2.4 GHz for the two-elevation cut-planes. The antenna has a maximum gain of 2.97 dBi.

For the experiment, the array is steered to $\left(\theta_s, \phi_s \right) = \left(0°, 0° \right)$ with a linear-polarized property, and a horizontal current distribution with binomial coefficients (1, 6, 15, 20, 15, 6, 1) is implemented along the array aperture while taking
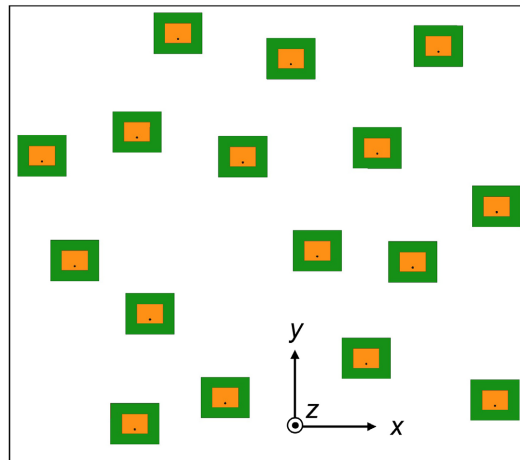
Figure 9. The front view of the sixteen-element volumetric random array modelled in HFSS.
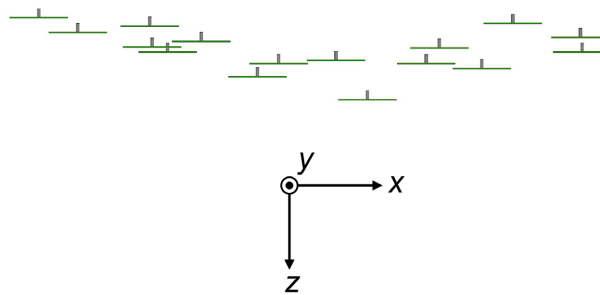

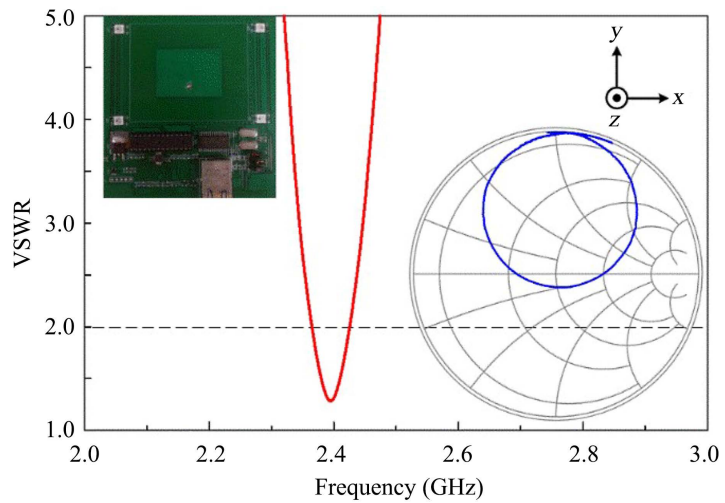**Figure 10.** The top view of the sixteen-element volumetric random array modelled in HFSS.

Figure 11. Measured VSWR and Smith Chart (overlaid) of the microstrip patch.

care of the depth difference. The experimental array is centered on a turntable during pattern measurements to avoid pattern distortion, and the 3-D beam-shaping result is examined from $\theta \geq -180°$ to $\theta \leq 180°$ in the *xz*-plane. Both measured and simulated results are evaluated at 2.4 GHz.

4. Result

The simulated and measured radiation patterns for tapering and non-tapering cases are plotted in Figure 13 and Figure 14, respectively. The tapering patterns are normalized to the non-tapering pattern for better comparison. Instead of focusing on the whole array's field-of-view ($-180° \leq \theta \leq 180°$), it is of particular interest for the range from $\theta \geq -30°$ to $\theta \leq 30°$ in the xz-plane, which allocated the first sidelobe. Figure 13 shows the simulated results, and the maximum gain (G_ϕ) is 22.47 dBi, located at the array's broadside ($\theta = 0°$). The peak of first sidelobe before tapering is 11.06 dBi at $\theta = -15°$, and it is 5.46 dBi at $\theta = 23°$ after tapering. A 5.6 dB sidelobe reduction is achieved, and the peak of first sidelobe moves away from the array's main beam. For measured patterns in Figure 14, the maximum gain (G_ϕ) is 22.47 dBi, located at the array's broadside ($\theta = 0°$). Before applying amplitude tapering, the peak of first sidelobe has gain of 12.49 dBi at $\theta = -12°$. After applying amplitude tapering, the peak of first sidelobe decreases to 2.76 dBi at $\theta = -25°$. There is a 9.73 dB sidelobe reduction after applying tapered weightings.
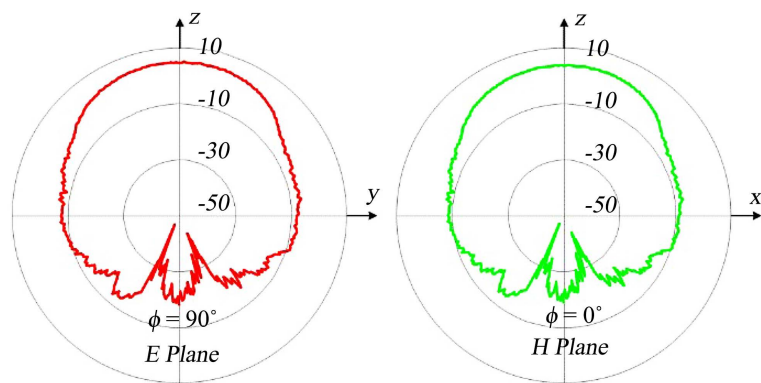

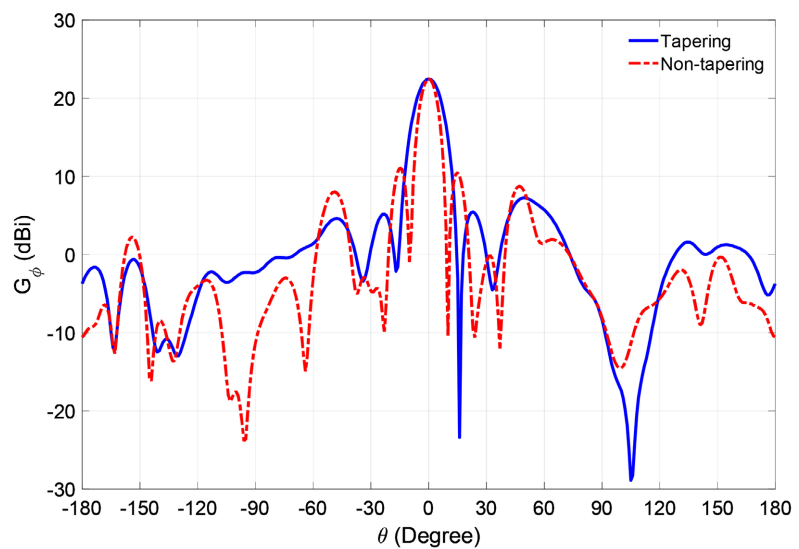**Figure 12.** Measured radiation pattern (dB) of the microstrip patch.

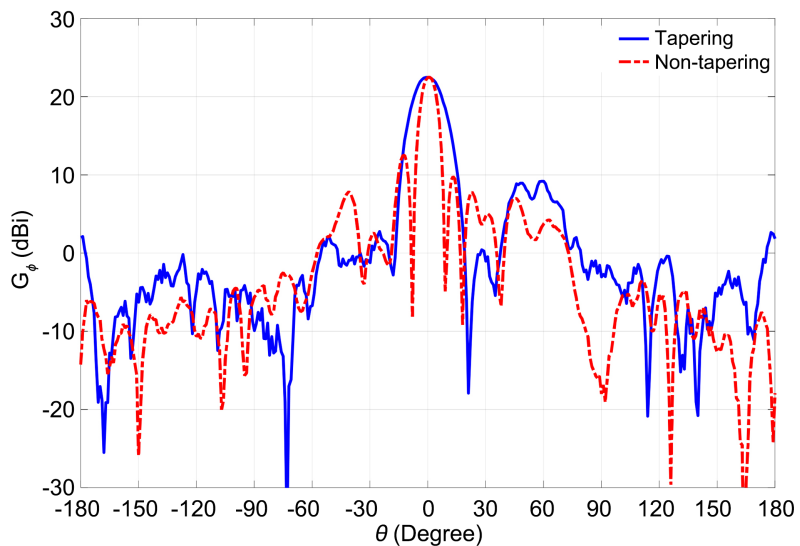**Figure 13.** The simulated patterns at f = 2.4 GHz in the xz-plane.

Figure 14. The measured patterns at f = 2.4 GHz in the *xz*-plane.

These results indicate that the amplitude tapering approach not only lowers the first sidelobe level but also pushes the first sidelobe away from the array's main beam. This method comes with the side effects of broader beamwidth, decreased directivity, and reduced aperture efficiency. After applying the tapering weightings, both simulated and measured SLLs are reduced. The measured results generally followed the expected behavior of the simulations. Even though the volumetric array is not aligned in the same plane, the proposed 3-D amplitude tapering technique deals with discontinuities of the current distribution along the array aperture well.

5. Conclusion

The emphasis of this work is on applications where the volumetric random array has only a few array elements, and sidelobes are needed to further suppress [12]-[22]. This paper clearly elaborates in 3-D amplitude tapering procedures and successfully demonstrates the beamshaping results. Simulated and measured radiation patterns of tapering and non-tapering are illustrated and compared to confirm the feasibility of the proposed 3-D beamshaping algorithm. It is observed that the array with tapering weightings has lower SLL and peak sidelobes moved away from the array's main beam.

Conflicts of Interest

The author declares no conflicts of interest regarding the publication of this paper.

References

[1] Jenn, D.C., Ryu, J.H., Yen-Chang, T. and Broadston, R. (2010) Adaptive Phase Synchronization in Distributed Digital Arrays. 2010 *NASA/ESA Conference on Adaptive Hardware and Systems*, Anaheim, 15-18 June 2010, 199-204.

https://doi.org/10.1109/AHS.2010.5546258

[2] Jenn, D., Loke, Y., Tong, M., Yeo, E.C. and Broadston, R. (2007) Distributed Phased Arrays with Wireless Beamforming. 2007 *Conference Record of the* 41*st Asilomar Conference on Signals*, *Systems and Computers*, Pacific Grove, 4-7 November 2007, 948-952. https://doi.org/10.1109/ACSSC.2007.4487359

[3] Yeh, S., Chen, Z. and Wu, Y. (2019) Developing Circular-Polarized Beamforming Techniques on Volumetric Random Arrays with Arbitrarily Oriented Array Elements. 2019 *International Symposium on Antennas and Propagation* (*ISAP*), Xi'an, 27-30 October 2019, 1-3.

[4] Yeh, S. and Chen, Z. (2021) Implementation of Beamforming a Circularly Polarized Radiation Pattern on 3D Random Arrays. 2020 *International Symposium on Antennas and Propagation* (*ISAP*), Osaka, 25-28 January 2021, 1-2. https://doi.org/10.23919/ISAP47053.2021.9391452

[5] Yeh, S. and Chen, Z. (2021) Beamforming a Circular-Polarized Radiation Pattern on Volumetric Random Arrays with Deliberately Aligned Array Antennas. *IEICE Communications Express*, **10**, 613-618. https://doi.org/10.1587/comex.2021SPL0020

[6] Sallam, T. and Attiya, A. (2017) Sidelobe Reduction and Resolution Enhancement by Random Perturbations in Periodic Antenna Arrays. 2017 *34th National Radio Science Conference* (*NRSC*), Alexandria, 13-16 March 2017, 49-55. https://doi.org/10.1109/NRSC.2017.7893476

[7] Buchanan, K. and Huff, G.H. (2014) A Stochastic Mathematical Framework for the Analysis of Spherically-Bound Random Arrays. *IEEE Transactions on Antennas and Propagation*, **62**, 3002-3011. https://doi.org/10.1109/TAP.2014.2313142

[8] Feng, B.-K. and Jenn, D.C. (2013) Grating Lobe Suppression for Distributed Digital Subarrays Using Virtual Filling. *IEEE Antennas and Wireless Propagation Letters*, **12**, 1323-1326. https://doi.org/10.1109/LAWP.2013.2285073

[9] Yeh, S. (2019) Investigating a Reversed-Field Sidelobe Cancelling Technique on Array Sidelobes Beamshaping. 2019 *8th Asia-Pacific Conference on Antennas and Propagation* (*APCAP*), Incheon, 4-7 August 2019, 588-589. https://doi.org/10.1109/APCAP47827.2019.9471975

[10] Yeh, S., Chamberland, J.-F. and Huff, G.H. (2017) An Investigation of Geolocation-Aware Beamforming Algorithms for Swarming UAVs. 2017 *IEEE International Symposium on Antennas and Propagation & USNC/URSI National Radio Science Meeting*, San Diego, 9-14 July 2017, 641-642. https://doi.org/10.1109/APUSNCURSINRSM.2017.8072363

[11] Jensen, J.S., Buchanan, K., Chamberland, J.-F. and Huff, G.H. (2017) A Computer Vision-Based Framework for the Synthesis and Analysis of Beamforming Behavior in Swarming Intelligent Systems. 2017 *IEEE Radar Conference* (*RadarConf*), Seattle, 8-12 May 2017, 118-122. https://doi.org/10.1109/RADAR.2017.7944182

[12] Yeh, S.-Y. (2018) Volumetric Random Phased Arrays and Their Applications. Doctoral Dissertation, Texas A & M University, College Station. https://hdl.handle.net/1969.1/173658

[13] Chen, Z., Yeh, S., Chamberland, J.-F. and Huff, G.H. (2019) A Sensor-Driven Analysis of Distributed Direction Finding Systems Based on UAV Swarms. *Sensors*, **19**, 2659. https://doi.org/10.3390/s19122659

[14] Yeh, S. (2018) A Phased Array Pattern Prediction Technique Based on the Pattern Multiplication Method. 2018 *Asia-Pacific Microwave Conference* (*APMC*), Kyoto, 6-9 November 2018, 1531-1533. https://doi.org/10.23919/APMC.2018.8617194

[15] Yeh, S. (2019) Beamshaping a Monopulse Array to Suppress Sidelobes for Both Sum

and Difference Beams. 2019 8*th Asia-Pacific Conference on Antennas and Propagation* (*APCAP*), Incheon, 4-7 August 2019, 42-43.
https://doi.org/10.1109/APCAP47827.2019.9472049

[16] Chen, Z., Yeh, S., Chamberland, J.-F. and Huff, G.H. (2020) Impact of Position Errors on Synthetic Aperture DOA Convergence Based on Swarming UAVs. 2020 *IEEE USNC-CNC-URSI North American Radio Science Meeting* (*Joint with AP-S Symposium*), Montreal, 5-10 July 2020, 83-84.
https://doi.org/10.23919/USNC/URSI49741.2020.9321600

[17] Yeh, S. and Chen, Z. (2019) Designing a Broadband Circularly Polarized Patch Antenna Array for Millimeter-Wave Beamforming. 2019 8*th Asia-Pacific Conference on Antennas and Propagation* (*APCAP*), Incheon, 4-7 August 2019, 205-206.
https://doi.org/10.1109/APCAP47827.2019.9472179

[18] Yeh, S. (2020) Designing a Subarray to Estimate Active Reflection Coefficients of an Infinite Array. 2020 9*th Asia-Pacific Conference on Antennas and Propagation* (*APCAP*), Xiamen, 4-7 August 2020, 1-2.
https://doi.org/10.1109/APCAP50217.2020.9246030

[19] Yeh, S. (2020) Beamforming a Holey-Plate Array with Random Circular Slots at Millimeter-Wave. 2020 9*th Asia-Pacific Conference on Antennas and Propagation* (*APCAP*), Xiamen, 4-7 August 2020, 1-2.
https://doi.org/10.1109/APCAP50217.2020.9245960

[20] Yeh, S. and Wu, Y. (2019) Leveraging Post-Processing Methodologies to Estimate Circular-Polarized Radiation Patterns of Phased Arrays. 2019 *International Symposium on Antennas and Propagation* (*ISAP*), Xi'an, 4-7 August 2020, 1-3.

[21] Yeh, S. and Huff, G.H. (2017) A Magnetless Duplex Retrodirective Patch Array with Phase Shifter for Signal Relay. 41*st Antenna Applications Symposium*, Monticello, IL, 20 September 2017, 53-74.

[22] Yeh, S. (2022) Periodic Linear Array with Uniformly Distributed Antennas. US Patent No. US20220166140A1.